



Differential branching fraction and angular analysis of the $B^+ \rightarrow K^+ \mu^+ \mu^-$ decay

The LHCb collaboration[†]

Abstract

The angular distribution and differential branching fraction of the decay $B^+ \rightarrow K^+ \mu^+ \mu^-$ are studied with a dataset corresponding to 1.0 fb^{-1} of integrated luminosity, collected by the LHCb experiment. The angular distribution is measured in bins of dimuon invariant mass squared and found to be consistent with Standard Model expectations. Integrating the differential branching fraction over the full dimuon invariant mass range yields a total branching fraction of $\mathcal{B}(B^+ \rightarrow K^+ \mu^+ \mu^-) = (4.36 \pm 0.15 \pm 0.18) \times 10^{-7}$. These measurements are the most precise to date of the $B^+ \rightarrow K^+ \mu^+ \mu^-$ decay.

To be submitted to Journal of High Energy Physics

[†]Authors are listed on the following pages.

LHCb collaboration

R. Aaij³⁸, C. Abellan Beteta^{33,n}, A. Adametz¹¹, B. Adeva³⁴, M. Adinolfi⁴³, C. Adrover⁶, A. Affolder⁴⁹, Z. Ajaltouni⁵, J. Albrecht³⁵, F. Alessio³⁵, M. Alexander⁴⁸, S. Ali³⁸, G. Alkhazov²⁷, P. Alvarez Cartelle³⁴, A.A. Alves Jr²², S. Amato², Y. Amhis³⁶, L. Anderlini^{17,f}, J. Anderson³⁷, R.B. Appleby⁵¹, O. Aquines Gutierrez¹⁰, F. Archilli^{18,35}, A. Artamonov³², M. Artuso⁵³, E. Aslanides⁶, G. Auriemma^{22,m}, S. Bachmann¹¹, J.J. Back⁴⁵, C. Baesso⁵⁴, W. Baldini¹⁶, R.J. Barlow⁵¹, C. Barschel³⁵, S. Barsuk⁷, W. Barter⁴⁴, A. Bates⁴⁸, Th. Bauer³⁸, A. Bay³⁶, J. Beddow⁴⁸, I. Bediaga¹, S. Belogurov²⁸, K. Belous³², I. Belyaev²⁸, E. Ben-Haim⁸, M. Benayoun⁸, G. Bencivenni¹⁸, S. Benson⁴⁷, J. Benton⁴³, A. Berezhnoy²⁹, R. Bernet³⁷, M.-O. Bettler⁴⁴, M. van Beuzekom³⁸, A. Bien¹¹, S. Bifani¹², T. Bird⁵¹, A. Bizzeti^{17,h}, P.M. Bjørnstad⁵¹, T. Blake³⁵, F. Blanc³⁶, C. Blanks⁵⁰, J. Blouw¹¹, S. Blusk⁵³, A. Bobrov³¹, V. Bocci²², A. Bondar³¹, N. Bondar²⁷, W. Bonivento¹⁵, S. Borghi^{48,51}, A. Borgia⁵³, T.J.V. Bowcock⁴⁹, E.E. Bowen^{46,37}, C. Bozzi¹⁶, T. Brambach⁹, J. van den Brand³⁹, J. Bressieux³⁶, D. Brett⁵¹, M. Britsch¹⁰, T. Britton⁵³, N.H. Brook⁴³, H. Brown⁴⁹, A. Büchler-Germann³⁷, I. Burducea²⁶, A. Bursche³⁷, J. Buytaert³⁵, S. Cadeddu¹⁵, O. Callot⁷, M. Calvi^{20,j}, M. Calvo Gomez^{33,n}, A. Camboni³³, P. Campana^{18,35}, A. Carbone^{14,c}, G. Carboni^{21,k}, R. Cardinale^{19,i}, A. Cardini¹⁵, L. Carson⁵⁰, K. Carvalho Akiba², G. Casse⁴⁹, M. Cattaneo³⁵, Ch. Cauet⁹, M. Charles⁵², Ph. Charpentier³⁵, P. Chen^{3,36}, N. Chiapolini³⁷, M. Chrzaszcz²³, K. Ciba³⁵, X. Cid Vidal³⁴, G. Ciezarek⁵⁰, P.E.L. Clarke⁴⁷, M. Clemencic³⁵, H.V. Cliff⁴⁴, J. Closier³⁵, C. Coca²⁶, V. Coco³⁸, J. Cogan⁶, E. Cogneras⁵, P. Collins³⁵, A. Comerma-Montells³³, A. Contu^{52,15}, A. Cook⁴³, M. Coombes⁴³, G. Corti³⁵, B. Couturier³⁵, G.A. Cowan³⁶, D. Craik⁴⁵, S. Cunliffe⁵⁰, R. Currie⁴⁷, C. D'Ambrosio³⁵, P. David⁸, P.N.Y. David³⁸, I. De Bonis⁴, K. De Bruyn³⁸, S. De Capua^{21,k}, M. De Cian³⁷, J.M. De Miranda¹, L. De Paula², P. De Simone¹⁸, D. Decamp⁴, M. Deckenhoff⁹, H. Degaudenzi^{36,35}, L. Del Buono⁸, C. Deplano¹⁵, D. Derkach¹⁴, O. Deschamps⁵, F. Dettori³⁹, A. Di Canto¹¹, J. Dickens⁴⁴, H. Dijkstra³⁵, P. Diniz Batista¹, F. Domingo Bonal^{33,n}, S. Donleavy⁴⁹, F. Dordel¹¹, A. Dosil Suárez³⁴, D. Dossett⁴⁵, A. Dovbnya⁴⁰, F. Dupertuis³⁶, R. Dzhelyadin³², A. Dziurda²³, A. Dzyuba²⁷, S. Easo⁴⁶, U. Egede⁵⁰, V. Egorychev²⁸, S. Eidelman³¹, D. van Eijk³⁸, S. Eisenhardt⁴⁷, R. Ekelhof⁹, L. Eklund⁴⁸, I. El Rifai⁵, Ch. Elsasser³⁷, D. Elsby⁴², D. Esperante Pereira³⁴, A. Falabella^{14,e}, C. Färber¹¹, G. Fardell⁴⁷, C. Farinelli³⁸, S. Farry¹², V. Fave³⁶, V. Fernandez Albor³⁴, F. Ferreira Rodrigues¹, M. Ferro-Luzzi³⁵, S. Filippov³⁰, C. Fitzpatrick³⁵, M. Fontana¹⁰, F. Fontanelli^{19,i}, R. Forty³⁵, O. Francisco², M. Frank³⁵, C. Frei³⁵, M. Frosini^{17,f}, S. Furcas²⁰, A. Gallas Torreira³⁴, D. Galli^{14,c}, M. Gandelman², P. Gandini⁵², Y. Gao³, J.-C. Garnier³⁵, J. Garofoli⁵³, J. Garra Tico⁴⁴, L. Garrido³³, C. Gaspar³⁵, R. Gauld⁵², E. Gersabeck¹¹, M. Gersabeck³⁵, T. Gershon^{45,35}, Ph. Ghez⁴, V. Gibson⁴⁴, V.V. Gligorov³⁵, C. Göbel⁵⁴, D. Golubkov²⁸, A. Golutvin^{50,28,35}, A. Gomes², H. Gordon⁵², M. Grabalosa Gándara³³, R. Graciani Diaz³³, L.A. Granado Cardoso³⁵, E. Graugés³³, G. Graziani¹⁷, A. Grecu²⁶, E. Greening⁵², S. Gregson⁴⁴, O. Grünberg⁵⁵, B. Gui⁵³, E. Gushchin³⁰, Yu. Guz³², T. Gys³⁵, C. Hadjivasiliou⁵³, G. Haefeli³⁶, C. Haen³⁵, S.C. Haines⁴⁴, S. Hall⁵⁰, T. Hampson⁴³, S. Hansmann-Menzemer¹¹, N. Harnew⁵², S.T. Harnew⁴³, J. Harrison⁵¹, P.F. Harrison⁴⁵, T. Hartmann⁵⁵, J. He⁷, V. Heijne³⁸, K. Hennessy⁴⁹, P. Henrard⁵, J.A. Hernando Morata³⁴, E. van Herwijnen³⁵, E. Hicks⁴⁹, D. Hill⁵², M. Hoballah⁵, P. Hopchev⁴, W. Hulsbergen³⁸, P. Hunt⁵², T. Huse⁴⁹, N. Hussain⁵², R.S. Huston¹², D. Hutchcroft⁴⁹, D. Hynds⁴⁸, V. Iakovenko⁴¹, P. Ilten¹², J. Imong⁴³, R. Jacobsson³⁵, A. Jaeger¹¹, M. Jahjah Hussein⁵, E. Jans³⁸, F. Jansen³⁸, P. Jatun³⁶, B. Jean-Marie⁷, F. Jing³, M. John⁵²,

D. Johnson⁵², C.R. Jones⁴⁴, B. Jost³⁵, M. Kaballo⁹, S. Kandybei⁴⁰, M. Karacson³⁵,
 T.M. Karbach⁹, J. Keaveney¹², I.R. Kenyon⁴², U. Kerzel³⁵, T. Ketel³⁹, A. Keune³⁶, B. Khanji²⁰,
 Y.M. Kim⁴⁷, O. Kochebina⁷, V. Komarov^{36,29}, R.F. Koopman³⁹, P. Koppenburg³⁸,
 M. Korolev²⁹, A. Kozlinskiy³⁸, L. Kravchuk³⁰, K. Kreplin¹¹, M. Kreps⁴⁵, G. Krocker¹¹,
 P. Krokovny³¹, F. Kruse⁹, M. Kucharczyk^{20,23,j}, V. Kudryavtsev³¹, T. Kvaratskheliya^{28,35},
 V.N. La Thi³⁶, D. Lacarrere³⁵, G. Lafferty⁵¹, A. Lai¹⁵, D. Lambert⁴⁷, R.W. Lambert³⁹,
 E. Lanciotti³⁵, G. Lanfranchi^{18,35}, C. Langenbruch³⁵, T. Latham⁴⁵, C. Lazzeroni⁴², R. Le Gac⁶,
 J. van Leerdam³⁸, J.-P. Lees⁴, R. Lefèvre⁵, A. Leflat^{29,35}, J. Lefrançois⁷, O. Leroy⁶, T. Lesiak²³,
 Y. Li³, L. Li Gioi⁵, M. Liles⁴⁹, R. Lindner³⁵, C. Linn¹¹, B. Liu³, G. Liu³⁵, J. von Loeben²⁰,
 J.H. Lopes², E. Lopez Asamar³³, N. Lopez-March³⁶, H. Lu³, J. Luisier³⁶, A. Mac Raighne⁴⁸,
 F. Machefert⁷, I.V. Machikhiliyan^{4,28}, F. Maciuc²⁶, O. Maev^{27,35}, J. Magnin¹, M. Maino²⁰,
 S. Malde⁵², G. Manca^{15,d}, G. Mancinelli⁶, N. Mangiafave⁴⁴, U. Marconi¹⁴, R. Märki³⁶,
 J. Marks¹¹, G. Martellotti²², A. Martens⁸, L. Martin⁵², A. Martín Sánchez⁷, M. Martinelli³⁸,
 D. Martinez Santos³⁵, A. Massafferri¹, Z. Mathe³⁵, C. Matteuzzi²⁰, M. Matveev²⁷, E. Maurice⁶,
 A. Mazurov^{16,30,35}, J. McCarthy⁴², G. McGregor⁵¹, R. McNulty¹², M. Meissner¹¹, M. Merk³⁸,
 J. Merkel⁹, D.A. Milanese¹³, M.-N. Minard⁴, J. Molina Rodriguez⁵⁴, S. Monteil⁵, D. Moran⁵¹,
 P. Morawski²³, R. Mountain⁵³, I. Mous³⁸, F. Muheim⁴⁷, K. Müller³⁷, R. Muresan²⁶, B. Muryn²⁴,
 B. Muster³⁶, J. Mylroie-Smith⁴⁹, P. Naik⁴³, T. Nakada³⁶, R. Nandakumar⁴⁶, I. Nasteva¹,
 M. Needham⁴⁷, N. Neufeld³⁵, A.D. Nguyen³⁶, C. Nguyen-Mau^{36,o}, M. Nicol⁷, V. Niess⁵,
 N. Nikitin²⁹, T. Nikodem¹¹, A. Nomerotski^{52,35}, A. Novoselov³², A. Oblakowska-Mucha²⁴,
 V. Obraztsov³², S. Oggero³⁸, S. Ogilvy⁴⁸, O. Okhrimenko⁴¹, R. Oldeman^{15,d,35}, M. Orlandea²⁶,
 J.M. Otalora Goicochea², P. Owen⁵⁰, B.K. Pal⁵³, A. Palano^{13,b}, M. Palutan¹⁸, J. Panman³⁵,
 A. Papanestis⁴⁶, M. Pappagallo⁴⁸, C. Parkes⁵¹, C.J. Parkinson⁵⁰, G. Passaleva¹⁷, G.D. Patel⁴⁹,
 M. Patel⁵⁰, G.N. Patrick⁴⁶, C. Patrignani^{19,i}, C. Pavel-Nicorescu²⁶, A. Pazos Alvarez³⁴,
 A. Pellegrino³⁸, G. Penso^{22,l}, M. Pepe Altarelli³⁵, S. Perazzini^{14,c}, D.L. Perego^{20,j},
 E. Perez Trigo³⁴, A. Pérez-Calero Yzquierdo³³, P. Perret⁵, M. Perrin-Terrin⁶, G. Pessina²⁰,
 K. Petridis⁵⁰, A. Petrolini^{19,i}, A. Phan⁵³, E. Picatoste Olloqui³³, B. Pie Valls³³, B. Pietrzyk⁴,
 T. Pilar⁴⁵, D. Pinci²², S. Playfer⁴⁷, M. Plo Casasus³⁴, F. Polci⁸, G. Polok²³, A. Poluektov^{45,31},
 E. Polcarpo², D. Popov¹⁰, B. Popovici²⁶, C. Potterat³³, A. Powell⁵², J. Prisciandaro³⁶,
 V. Pugatch⁴¹, A. Puig Navarro³⁶, W. Qian³, J.H. Rademacker⁴³, B. Rakotomiaramanana³⁶,
 M.S. Rangel², I. Raniuk⁴⁰, N. Rauschmayr³⁵, G. Raven³⁹, S. Redford⁵², M.M. Reid⁴⁵,
 A.C. dos Reis¹, S. Ricciardi⁴⁶, A. Richards⁵⁰, K. Rinnert⁴⁹, V. Rives Molina³³,
 D.A. Roa Romero⁵, P. Robbe⁷, E. Rodrigues^{48,51}, P. Rodriguez Perez³⁴, G.J. Rogers⁴⁴,
 S. Roiser³⁵, V. Romanovsky³², A. Romero Vidal³⁴, J. Rouvinet³⁶, T. Ruf³⁵, H. Ruiz³³,
 G. Sabatino^{21,k}, J.J. Saborido Silva³⁴, N. Sagidova²⁷, P. Sail⁴⁸, B. Saitta^{15,d}, C. Salzmann³⁷,
 B. Sanmartin Sedes³⁴, M. Sannino^{19,i}, R. Santacesaria²², C. Santamarina Rios³⁴, R. Santinelli³⁵,
 E. Santovetti^{21,k}, M. Sapunov⁶, A. Sarti^{18,l}, C. Satriano^{22,m}, A. Satta²¹, M. Savrie^{16,e},
 P. Schaack⁵⁰, M. Schiller³⁹, H. Schindler³⁵, S. Schleich⁹, M. Schlupp⁹, M. Schmelling¹⁰,
 B. Schmidt³⁵, O. Schneider³⁶, A. Schopper³⁵, M.-H. Schune⁷, R. Schwemmer³⁵, B. Sciascia¹⁸,
 A. Sciubba^{18,l}, M. Seco³⁴, A. Semennikov²⁸, K. Senderowska²⁴, I. Sepp⁵⁰, N. Serra³⁷,
 J. Serrano⁶, P. Seyfert¹¹, M. Shapkin³², I. Shapoval^{40,35}, P. Shatalov²⁸, Y. Shcheglov²⁷,
 T. Shears^{49,35}, L. Shekhtman³¹, O. Shevchenko⁴⁰, V. Shevchenko²⁸, A. Shires⁵⁰,
 R. Silva Coutinho⁴⁵, T. Skwarnicki⁵³, N.A. Smith⁴⁹, E. Smith^{52,46}, M. Smith⁵¹, K. Sobczak⁵,
 F.J.P. Soler⁴⁸, A. Solomin⁴³, F. Soomro^{18,35}, D. Souza⁴³, B. Souza De Paula², B. Spaan⁹,
 A. Sparkes⁴⁷, P. Spradlin⁴⁸, F. Stagni³⁵, S. Stahl¹¹, O. Steinkamp³⁷, S. Stoica²⁶, S. Stone⁵³,
 B. Storaci³⁸, M. Straticiuc²⁶, U. Straumann³⁷, V.K. Subbiah³⁵, S. Swientek⁹, M. Szczekowski²⁵,

P. Szczypka^{36,35}, T. Szumlak²⁴, S. T'Jampens⁴, M. Teklishyn⁷, E. Teodorescu²⁶, F. Teubert³⁵, C. Thomas⁵², E. Thomas³⁵, J. van Tilburg¹¹, V. Tisserand⁴, M. Tobin³⁷, S. Tolks³⁹, S. Topp-Joergensen⁵², N. Torr⁵², E. Tournefier^{4,50}, S. Tourneur³⁶, M.T. Tran³⁶, A. Tsaregorodtsev⁶, N. Tuning³⁸, M. Ubeda Garcia³⁵, A. Ukleja²⁵, D. Urner⁵¹, U. Uwer¹¹, V. Vagnoni¹⁴, G. Valenti¹⁴, R. Vazquez Gomez³³, P. Vazquez Regueiro³⁴, S. Vecchi¹⁶, J.J. Velthuis⁴³, M. Veltri^{17,g}, G. Veneziano³⁶, M. Vesterinen³⁵, B. Viaud⁷, I. Videau⁷, D. Vieira², X. Vilasis-Cardona^{33,n}, J. Visniakov³⁴, A. Vollhardt³⁷, D. Volyanskyy¹⁰, D. Voong⁴³, A. Vorobyev²⁷, V. Vorobyev³¹, H. Voss¹⁰, C. Voß⁵⁵, R. Waldi⁵⁵, R. Wallace¹², S. Wandernoth¹¹, J. Wang⁵³, D.R. Ward⁴⁴, N.K. Watson⁴², A.D. Webber⁵¹, D. Websdale⁵⁰, M. Whitehead⁴⁵, J. Wicht³⁵, D. Wiedner¹¹, L. Wiggers³⁸, G. Wilkinson⁵², M.P. Williams^{45,46}, M. Williams^{50,p}, F.F. Wilson⁴⁶, J. Wishahi⁹, M. Witek^{23,35}, W. Witzeling³⁵, S.A. Wotton⁴⁴, S. Wright⁴⁴, S. Wu³, K. Wyllie³⁵, Y. Xie⁴⁷, F. Xing⁵², Z. Xing⁵³, Z. Yang³, R. Young⁴⁷, X. Yuan³, O. Yushchenko³², M. Zangoli¹⁴, M. Zavertyaev^{10,a}, F. Zhang³, L. Zhang⁵³, W.C. Zhang¹², Y. Zhang³, A. Zhelezov¹¹, L. Zhong³, A. Zvyagin³⁵.

¹ *Centro Brasileiro de Pesquisas Físicas (CBPF), Rio de Janeiro, Brazil*

² *Universidade Federal do Rio de Janeiro (UFRJ), Rio de Janeiro, Brazil*

³ *Center for High Energy Physics, Tsinghua University, Beijing, China*

⁴ *LAPP, Université de Savoie, CNRS/IN2P3, Annecy-Le-Vieux, France*

⁵ *Clermont Université, Université Blaise Pascal, CNRS/IN2P3, LPC, Clermont-Ferrand, France*

⁶ *CPPM, Aix-Marseille Université, CNRS/IN2P3, Marseille, France*

⁷ *LAL, Université Paris-Sud, CNRS/IN2P3, Orsay, France*

⁸ *LPNHE, Université Pierre et Marie Curie, Université Paris Diderot, CNRS/IN2P3, Paris, France*

⁹ *Fakultät Physik, Technische Universität Dortmund, Dortmund, Germany*

¹⁰ *Max-Planck-Institut für Kernphysik (MPIK), Heidelberg, Germany*

¹¹ *Physikalisches Institut, Ruprecht-Karls-Universität Heidelberg, Heidelberg, Germany*

¹² *School of Physics, University College Dublin, Dublin, Ireland*

¹³ *Sezione INFN di Bari, Bari, Italy*

¹⁴ *Sezione INFN di Bologna, Bologna, Italy*

¹⁵ *Sezione INFN di Cagliari, Cagliari, Italy*

¹⁶ *Sezione INFN di Ferrara, Ferrara, Italy*

¹⁷ *Sezione INFN di Firenze, Firenze, Italy*

¹⁸ *Laboratori Nazionali dell'INFN di Frascati, Frascati, Italy*

¹⁹ *Sezione INFN di Genova, Genova, Italy*

²⁰ *Sezione INFN di Milano Bicocca, Milano, Italy*

²¹ *Sezione INFN di Roma Tor Vergata, Roma, Italy*

²² *Sezione INFN di Roma La Sapienza, Roma, Italy*

²³ *Henryk Niewodniczanski Institute of Nuclear Physics Polish Academy of Sciences, Kraków, Poland*

²⁴ *AGH University of Science and Technology, Kraków, Poland*

²⁵ *National Center for Nuclear Research (NCBJ), Warsaw, Poland*

²⁶ *Horia Hulubei National Institute of Physics and Nuclear Engineering, Bucharest-Magurele, Romania*

²⁷ *Petersburg Nuclear Physics Institute (PNPI), Gatchina, Russia*

²⁸ *Institute of Theoretical and Experimental Physics (ITEP), Moscow, Russia*

²⁹ *Institute of Nuclear Physics, Moscow State University (SINP MSU), Moscow, Russia*

³⁰ *Institute for Nuclear Research of the Russian Academy of Sciences (INR RAN), Moscow, Russia*

³¹ *Budker Institute of Nuclear Physics (SB RAS) and Novosibirsk State University, Novosibirsk, Russia*

³² *Institute for High Energy Physics (IHEP), Protvino, Russia*

³³ *Universitat de Barcelona, Barcelona, Spain*

³⁴ *Universidad de Santiago de Compostela, Santiago de Compostela, Spain*

³⁵ *European Organization for Nuclear Research (CERN), Geneva, Switzerland*

- ³⁶ *Ecole Polytechnique Fédérale de Lausanne (EPFL), Lausanne, Switzerland*
- ³⁷ *Physik-Institut, Universität Zürich, Zürich, Switzerland*
- ³⁸ *Nikhef National Institute for Subatomic Physics, Amsterdam, The Netherlands*
- ³⁹ *Nikhef National Institute for Subatomic Physics and VU University Amsterdam, Amsterdam, The Netherlands*
- ⁴⁰ *NSC Kharkiv Institute of Physics and Technology (NSC KIPT), Kharkiv, Ukraine*
- ⁴¹ *Institute for Nuclear Research of the National Academy of Sciences (KINR), Kyiv, Ukraine*
- ⁴² *University of Birmingham, Birmingham, United Kingdom*
- ⁴³ *H.H. Wills Physics Laboratory, University of Bristol, Bristol, United Kingdom*
- ⁴⁴ *Cavendish Laboratory, University of Cambridge, Cambridge, United Kingdom*
- ⁴⁵ *Department of Physics, University of Warwick, Coventry, United Kingdom*
- ⁴⁶ *STFC Rutherford Appleton Laboratory, Didcot, United Kingdom*
- ⁴⁷ *School of Physics and Astronomy, University of Edinburgh, Edinburgh, United Kingdom*
- ⁴⁸ *School of Physics and Astronomy, University of Glasgow, Glasgow, United Kingdom*
- ⁴⁹ *Oliver Lodge Laboratory, University of Liverpool, Liverpool, United Kingdom*
- ⁵⁰ *Imperial College London, London, United Kingdom*
- ⁵¹ *School of Physics and Astronomy, University of Manchester, Manchester, United Kingdom*
- ⁵² *Department of Physics, University of Oxford, Oxford, United Kingdom*
- ⁵³ *Syracuse University, Syracuse, NY, United States*
- ⁵⁴ *Pontificia Universidade Católica do Rio de Janeiro (PUC-Rio), Rio de Janeiro, Brazil, associated to ²*
- ⁵⁵ *Institut für Physik, Universität Rostock, Rostock, Germany, associated to ¹¹*
- ^a *P.N. Lebedev Physical Institute, Russian Academy of Science (LPI RAS), Moscow, Russia*
- ^b *Università di Bari, Bari, Italy*
- ^c *Università di Bologna, Bologna, Italy*
- ^d *Università di Cagliari, Cagliari, Italy*
- ^e *Università di Ferrara, Ferrara, Italy*
- ^f *Università di Firenze, Firenze, Italy*
- ^g *Università di Urbino, Urbino, Italy*
- ^h *Università di Modena e Reggio Emilia, Modena, Italy*
- ⁱ *Università di Genova, Genova, Italy*
- ^j *Università di Milano Bicocca, Milano, Italy*
- ^k *Università di Roma Tor Vergata, Roma, Italy*
- ^l *Università di Roma La Sapienza, Roma, Italy*
- ^m *Università della Basilicata, Potenza, Italy*
- ⁿ *LIFAEELS, La Salle, Universitat Ramon Llull, Barcelona, Spain*
- ^o *Hanoi University of Science, Hanoi, Viet Nam*
- ^p *Massachusetts Institute of Technology, Cambridge, MA, United States*

1 Introduction

The $B^+ \rightarrow K^+ \mu^+ \mu^-$ decay¹ is a $b \rightarrow s$ flavour changing neutral current process that is mediated in the Standard Model (SM) by electroweak box and penguin diagrams. In many well motivated extensions to the SM, new particles can enter in competing loop diagrams, modifying the branching fraction of the decay or the angular distribution of the dimuon system. The differential decay rate of the B^+ (B^-) decay, as a function of $\cos \theta_\ell$, the cosine of the angle between the μ^- (μ^+) and the K^+ (K^-) in the rest frame of the dimuon system, can be written as

$$\frac{1}{\Gamma} \frac{d\Gamma[B^+ \rightarrow K^+ \mu^+ \mu^-]}{d\cos \theta_\ell} = \frac{3}{4}(1 - F_H)(1 - \cos^2 \theta_\ell) + \frac{1}{2}F_H + A_{\text{FB}} \cos \theta_\ell, \quad (1)$$

which depends on two parameters, the forward-backward asymmetry of the dimuon system, A_{FB} , and the parameter F_H [1,2]. If muons were massless, F_H would be proportional to the contributions from (pseudo-)scalar and tensor operators to the partial width, Γ . The partial width, A_{FB} and F_H are functions of the dimuon invariant mass squared ($q^2 = m_{\mu^+ \mu^-}^2$).

In contrast to the case of the $B^0 \rightarrow K^{*0} \mu^+ \mu^-$ [3] decay, A_{FB} is zero for $B^+ \rightarrow K^+ \mu^+ \mu^-$ in the SM. Any non-zero value for A_{FB} would point to a contribution from new particles that would extend the set of SM operators. In models with (pseudo-)scalar or tensor-like couplings $|A_{\text{FB}}|$ can be enhanced by up to 15% [2,4]. Similarly, F_H is close to zero in the SM (see Fig. 3), but can be enhanced in new physics models, with (pseudo-)scalar or tensor-like couplings, up to $F_H \lesssim 0.5$. Recent predictions for these parameters in the SM are described in Refs. [2,5,6]. Any physics model has to satisfy the constraint $|A_{\text{FB}}| \leq F_H/2$ for Eq. (1) to stay positive in all regions of phase space. The contributions of scalar and pseudoscalar operators to A_{FB} and F_H are constrained by recent limits on the branching fraction of $B_s^0 \rightarrow \mu^+ \mu^-$ [7]. The differential branching fraction of $B^+ \rightarrow K^+ \mu^+ \mu^-$ can be used to constrain the contributions from (axial-)vector couplings in the SM operator basis [6,8,9].

The relative decay rate of $B^+ \rightarrow K^+ \mu^+ \mu^-$ to $B^0 \rightarrow K^0 \mu^+ \mu^-$ has previously been studied by the LHCb collaboration in the context of a measurement of the isospin asymmetry [10]. This paper presents a measurement of the differential branching fraction ($d\mathcal{B}/dq^2$), F_H and A_{FB} of the decay $B^+ \rightarrow K^+ \mu^+ \mu^-$ in seven bins of q^2 and a measurement of the total branching fraction. The analysis is based on 1.0 fb^{-1} of integrated luminosity collected in $\sqrt{s} = 7 \text{ TeV}$ pp collisions by the LHCb experiment in 2011.

2 Experimental setup

The LHCb detector [11] is a single-arm forward spectrometer, covering the pseudorapidity range $2 < \eta < 5$, that is designed to study b and c hadron decays. A dipole magnet with a bending power of 4 Tm and a large area tracking detector provide a momentum resolution ranging from 0.4% for tracks with a momentum of 5 GeV/ c to 0.6% for a momentum of

¹Charge conjugation is implied throughout this paper unless explicitly stated otherwise.

100 GeV/c. A silicon micro-strip detector, located around the pp interaction region, provides excellent separation of B meson decay vertices from the primary pp interaction and an impact parameter resolution of 20 μm for tracks with high transverse momentum (p_{T}). Two ring-imaging Cherenkov (RICH) detectors provide kaon-pion separation in the momentum range 2 – 100 GeV/c. Muons are identified based on hits created in a system of multiwire proportional chambers interleaved with iron filters. The LHCb trigger comprises a hardware trigger and a two-stage software trigger that performs a full event reconstruction.

Samples of simulated events are used to estimate the contribution from specific sources of exclusive backgrounds and the efficiency to trigger, reconstruct and select the $B^+ \rightarrow K^+ \mu^+ \mu^-$ signal. The simulated pp interactions are generated using PYTHIA 6.4 [12] with a specific LHCb configuration [13]. Decays of hadronic particles are then described by EVTGEN [14] in which final state radiation is generated using PHOTOS [15]. Finally, the GEANT4 toolkit [16] is used to simulate the detector response to the particles produced by PYTHIA/EVTGEN, as described in Ref. [17]. The simulated samples are corrected for differences between data and simulation in the B^+ momentum spectrum, the detector impact parameter resolution, particle identification and tracking system performance.

3 Selection of signal candidates

The $B^+ \rightarrow K^+ \mu^+ \mu^-$ candidates are selected from events that have been triggered by a single high transverse-momentum muon, with $p_{\text{T}} > 1.5$ GeV/c, in the hardware trigger. In the first stage of the software trigger, candidates are selected if there is a reconstructed track in the event with high impact parameter with respect to the primary pp interaction and high p_{T} [18]. In the second stage of the software trigger, candidates are triggered on the kinematic properties of the partially or fully reconstructed B^+ candidate [19].

Signal candidates are then selected for further analysis based on the following requirements: the B^+ decay vertex is separated from the primary pp interaction; the B^+ candidate impact parameter is small, and the kaon and muon impact parameters large, with respect to the primary pp interaction; the B^+ candidate momentum vector points along the B^+ line of flight to one of the primary pp interactions in the event.

A tighter multivariate selection, using a Boosted Decision Tree (BDT) [20] with the AdaBoost algorithm [21], is then applied to select a clean sample of $B^+ \rightarrow K^+ \mu^+ \mu^-$ candidates. The BDT uses kinematic variables including the reconstructed B^+ decay time, the angle between the B^+ line of flight and the B^+ momentum vector, the quality of the vertex fit of the reconstructed B^+ candidate, impact parameter (with respect to the primary pp interaction) and p_{T} of the B^+ and muons and the track quality of the kaon. The variables that are used in the BDT provide good separating power between signal and background, while minimising acceptance effects in q^2 and $\cos \theta_{\ell}$ that could bias the differential branching fraction, $A_{\text{FB}}(q^2)$ or $F_{\text{H}}(q^2)$. The multivariate selection is trained on data, using $B^+ \rightarrow K^+ J/\psi$ ($J/\psi \rightarrow \mu^+ \mu^-$) candidates as a proxy for the signal and $B^+ \rightarrow K^+ \mu^+ \mu^-$ candidates from the upper mass sideband ($5350 < m_{K^+ \mu^+ \mu^-} < 5600$ MeV/c²) for the background. The training and testing of the BDT is carried out

using a data sample corresponding to 0.1 fb^{-1} of integrated luminosity, that is not used in the subsequent analysis. The BDT selection is 85 – 90% (depending on q^2) efficient on simulated candidates that have passed the earlier selection.

Finally, a neural network, using information from the RICH [22], calorimeters and muon system is used to reject backgrounds where a pion is incorrectly identified as the kaon from the $B^+ \rightarrow K^+ \mu^+ \mu^-$ decay. The network is trained on simulated event samples to give the posterior probability for charged hadrons to be correctly identified. The particle identification performance of the network is calibrated using pions and kaons from the decay chain $D^{*+} \rightarrow D^0 (\rightarrow K^- \pi^+) \pi^+$ in the data. Based on simulation, the efficiency of the neural network particle identification requirement is estimated to be $\gtrsim 95\%$ on the signal.

The contribution from combinatorial backgrounds, where the reconstructed K^+ , μ^+ and μ^- do not come from the same b -hadron decay, is reduced to a small level by the multivariate selection. Remaining backgrounds come from exclusive b -hadron decays. The decays $B^+ \rightarrow K^+ J/\psi$ and $B^+ \rightarrow K^+ \psi(2S)$ are rejected by removing the regions of dimuon invariant mass around the charmonium resonances ($2946 < m_{\mu^+ \mu^-} < 3176 \text{ MeV}/c^2$ and $3586 < m_{\mu^+ \mu^-} < 3776 \text{ MeV}/c^2$). Candidates with $m_{K^+ \mu^+ \mu^-} < 5170 \text{ MeV}/c^2$ were also removed to reject backgrounds from partially reconstructed B decays, such as $B^0 \rightarrow K^{*0} \mu^+ \mu^-$. The potential background from $B^+ \rightarrow K^+ J/\psi$ ($J/\psi \rightarrow \mu^+ \mu^-$), where the kaon is identified as a muon and a muon as the kaon, is reduced by requiring that the kaon candidate fails the muon identification criteria if the $K^+ \mu^-$ mass is consistent with that of the J/ψ or $\psi(2S)$. Candidates with a $K^+ \mu^-$ mass consistent with coming from a misidentified $\bar{D}^0 \rightarrow K^+ \pi^-$ decay are rejected to remove contributions from $B^+ \rightarrow \bar{D}^0 \pi^+$. After the application of all of the selection criteria, the dominant sources of exclusive background are $B^+ \rightarrow K^+ \pi^- \pi^+$ [23] and $B^+ \rightarrow \pi^+ \mu^+ \mu^-$ [24]. These are determined from simulation to be at the level of $(1.5 \pm 0.7)\%$ and $(1.2 \pm 0.2)\%$ of the signal, respectively.

4 Differential and total branching fraction

The $K^+ \mu^+ \mu^-$ invariant mass distribution of the selected $B^+ \rightarrow K^+ \mu^+ \mu^-$ candidates is shown in Fig. 1. The number of signal candidates is estimated by performing an extended unbinned maximum likelihood fit to the $K^+ \mu^+ \mu^-$ invariant mass distribution of the selected candidates. The signal line-shape is extracted from a fit to a $B^+ \rightarrow K^+ J/\psi$ ($J/\psi \rightarrow \mu^+ \mu^-$) control sample (which is two orders of magnitude larger than the signal sample), and is parameterised by the sum of two Crystal Ball functions [25]. The combinatorial background is parameterised by a slowly falling exponential distribution. Contributions from $B^+ \rightarrow K^+ \pi^+ \pi^-$ and $B^+ \rightarrow \pi^+ \mu^+ \mu^-$ decays are included in the fit. The line shapes of these peaking backgrounds are taken from simulated events. In total, 1232 ± 40 $B^+ \rightarrow K^+ \mu^+ \mu^-$ signal candidates are observed in the $0.05 < q^2 < 22.00 \text{ GeV}^2/c^4$ range. The yields in each of the q^2 bins used in the subsequent analysis are shown in Table 1.

The differential branching fraction in each of the q^2 bins is estimated by normalising the

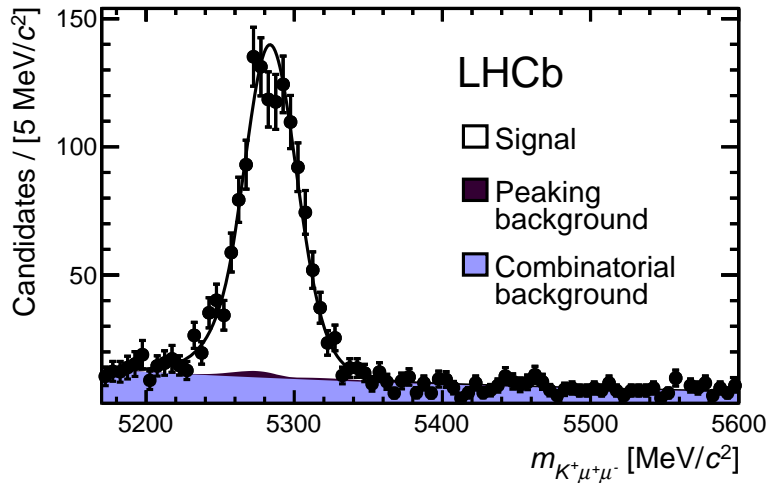


Figure 1: Invariant mass of selected $B^+ \rightarrow K^+ \mu^+ \mu^-$ candidates with $0.05 < q^2 < 22.00 \text{ GeV}^2/c^4$. Candidates with a dimuon invariant mass consistent with that of the J/ψ or $\psi(2S)$ are excluded. The peaking background contribution from the decays $B^+ \rightarrow K^+ \pi^+ \pi^-$ and $B^+ \rightarrow \pi^+ \mu^+ \mu^-$ is indicated in the figure.

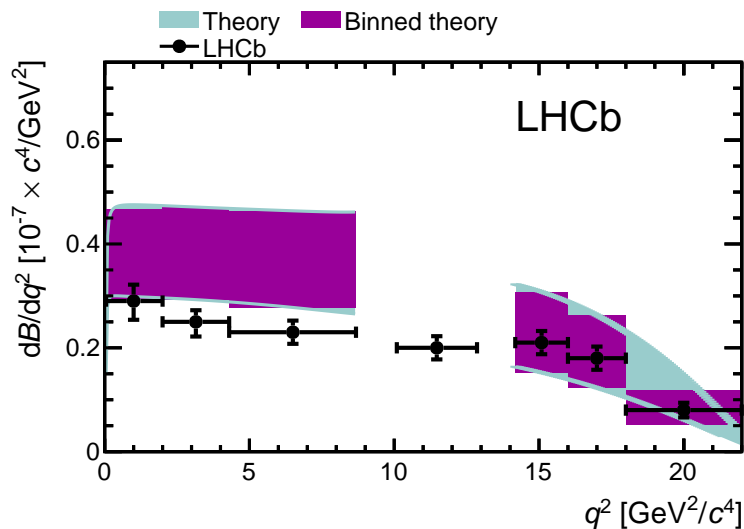


Figure 2: Differential branching fraction of $B^+ \rightarrow K^+ \mu^+ \mu^-$ as a function of the dimuon invariant mass squared, q^2 . The SM theory prediction (see text) is given as the continuous cyan (light) band and the rate-average of this prediction across the q^2 bin is indicated by the purple (dark) region. No SM prediction is included for the regions close to the narrow $c\bar{c}$ resonances.

$B^+ \rightarrow K^+ \mu^+ \mu^-$ event yield, N_{sig} , in the q^2 bin to the total event yield of the $B^+ \rightarrow K^+ J/\psi$ sample, $N_{K^+ J/\psi}$, and correcting for the relative efficiency between the two decays in the q^2 bin, $\varepsilon_{K^+ J/\psi} / \varepsilon_{K^+ \mu^+ \mu^-}$,

$$\frac{d\mathcal{B}}{dq^2} = \frac{1}{q_{\text{max}}^2 - q_{\text{min}}^2} \frac{N_{\text{sig}}}{N_{K^+ J/\psi}} \frac{\varepsilon_{K^+ J/\psi}}{\varepsilon_{K^+ \mu^+ \mu^-}} \times \mathcal{B}(B^+ \rightarrow K^+ J/\psi) \times \mathcal{B}(J/\psi \rightarrow \mu^+ \mu^-). \quad (2)$$

The branching fractions of $B^+ \rightarrow K^+ J/\psi$ and $J/\psi \rightarrow \mu^+ \mu^-$ are $\mathcal{B}(B^+ \rightarrow K^+ J/\psi) = (1.014 \pm 0.034) \times 10^{-3}$ and $\mathcal{B}(J/\psi \rightarrow \mu^+ \mu^-) = (5.93 \pm 0.06) \times 10^{-2}$ [26]. The resulting differential branching fraction is shown in Fig. 2.

The bands shown in Fig. 2 indicate the theoretical prediction for the differential branching fraction and are calculated using input from Refs. [6] and [27]. In the low q^2 region, the calculations are based on QCD factorisation and soft collinear effective theory (SCET) [28], which profit from having a heavy B^+ meson and an energetic kaon. In the soft-recoil, high q^2 region, an operator product expansion (OPE) is used to estimate the long-distance contributions from quark loops [29, 30]. No theory prediction is included in the region close to the narrow $c\bar{c}$ resonances (the J/ψ and $\psi(2S)$) where the assumptions from QCD factorisation/SCET and the OPE break down. The form-factor calculations are taken from Ref. [31]. A dimensional estimate is made on the uncertainty on the decay amplitudes from QCD factorisation/SCET [32].

The total branching fraction is measured to be

$$\mathcal{B}(B^+ \rightarrow K^+ \mu^+ \mu^-) = (4.36 \pm 0.15 \pm 0.18) \times 10^{-7},$$

by summing over the partial branching fractions and accounting for the q^2 regions that are not used in the differential branching fraction analysis. These regions account for $\sim 14.3\%$ of the total branching fraction (no uncertainty is assigned to this number). This estimate ignores long distance effects and uses a model for $d\Gamma/dq^2$ described in Ref. [1] to extrapolate across the $c\bar{c}$ resonance region. The values of the Wilson coefficients and the form-factors used in this model have been updated according to Refs. [33] and [31].

5 Angular analysis

In each bin of q^2 , A_{FB} and F_{H} are estimated by performing a simultaneous unbinned maximum likelihood fit to the $K^+ \mu^+ \mu^-$ invariant mass and $\cos\theta_\ell$ distribution of the B^+ candidates. The candidates are weighted to account for the effects of the detector reconstruction, trigger and the event selection. The weights are derived from a SM simulation of the $B^+ \rightarrow K^+ \mu^+ \mu^-$ decay in bins of width $0.5 \text{ GeV}^2/c^4$ in q^2 and 0.1 in $\cos\theta_\ell$. This binning is investigated as a potential source of systematic uncertainty. The largest weights (and largest acceptance effects) apply to events with extreme values of $\cos\theta_\ell$ ($|\cos\theta_\ell| \sim 1$) at low q^2 . This distortion arises mainly from the requirement for a muon to have $p \gtrsim 3 \text{ GeV}/c$ to reach the LHCb muon system. This effect is well modelled in the simulation.

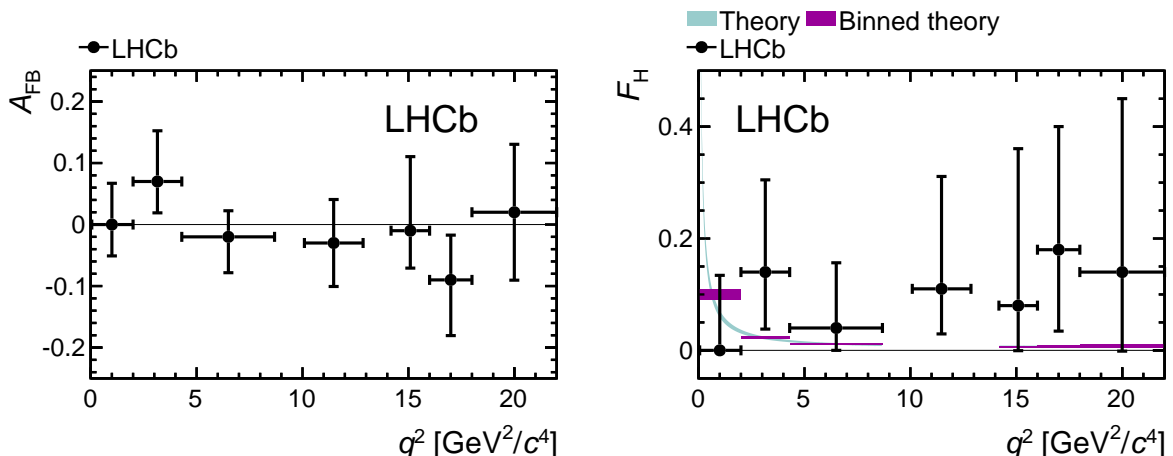


Figure 3: Dimuon forward-backward asymmetry, A_{FB} , and the parameter F_{H} for $B^+ \rightarrow K^+ \mu^+ \mu^-$ as a function of the dimuon invariant mass squared, q^2 . The SM theory prediction (see text) for F_{H} is given as the continuous cyan (light) band and the rate-average of this prediction across the q^2 bin is indicated by the purple (dark) region. No SM prediction is included for the regions close to the narrow $c\bar{c}$ resonances.

Equation (1) is used to describe the signal angular distribution. The background angular and mass shapes are treated as independent in the fit. The angular distribution of the background is parameterised by a second-order Chebychev polynomial, which is observed to describe well the background away from the signal mass window ($5230 < m_{K^+ \mu^+ \mu^-} < 5330 \text{ MeV}/c^2$).

The resulting values of A_{FB} and F_{H} in the bins of q^2 are indicated in Fig. 3 and in Table 1. The measured values of A_{FB} are consistent with the SM expectation of zero asymmetry. The 68% confidence intervals on A_{FB} and F_{H} are estimated using pseudo-experiments and the Feldman-Cousins technique [34]. This avoids potential biases in the estimate of the parameter uncertainties that come from using event weights in the likelihood fit or from the boundary condition ($|A_{\text{FB}}| \leq F_{\text{H}}/2$). When estimating the uncertainty on A_{FB} (F_{H}), F_{H} (A_{FB}) is treated as a nuisance parameter (along with the background parameters in the fit). The maximum-likelihood estimate of the nuisance parameters is used when generating the pseudo-experiments. The resulting confidence intervals ignore correlations between A_{FB} and F_{H} and are not simultaneously valid at the 68% confidence level.

6 Systematic uncertainties

For the differential branching fraction measurement, the largest source of systematic uncertainty comes from an uncertainty of $\sim 4\%$ on the $B^+ \rightarrow K^+ J/\psi$ and $J/\psi \rightarrow \mu^+ \mu^-$ branching fractions [26]. The systematic uncertainties are largely correlated between the q^2

Table 1: Signal yield (N_{sig}), differential branching fraction ($d\mathcal{B}/dq^2$), the parameter F_{H} and dimuon forward-backward asymmetry (A_{FB}) for the $B^+ \rightarrow K^+ \mu^+ \mu^-$ decay in the q^2 bins used in the analysis. Results are also given in the $1 < q^2 < 6 \text{ GeV}^2/c^4$ range where theoretical uncertainties are best under control.

q^2 (GeV^2/c^4)	N_{sig}	$d\mathcal{B}/dq^2$ ($10^{-8} \text{ GeV}^{-2}c^4$)	F_{H}	A_{FB}
0.05 – 2.00	159 ± 14	$2.85 \pm 0.27 \pm 0.14$	$0.00^{+0.12}_{-0.00}^{+0.06}_{-0.00}$	$0.00^{+0.06}_{-0.05}^{+0.03}_{-0.01}$
2.00 – 4.30	164 ± 14	$2.49 \pm 0.23 \pm 0.10$	$0.14^{+0.16}_{-0.10}^{+0.04}_{-0.02}$	$0.07^{+0.08}_{-0.05}^{+0.02}_{-0.01}$
4.30 – 8.68	327 ± 20	$2.29 \pm 0.16 \pm 0.09$	$0.04^{+0.10}_{-0.04}^{+0.06}_{-0.04}$	$-0.02^{+0.03}_{-0.05}^{+0.03}_{-0.03}$
10.09 – 12.86	211 ± 17	$2.04 \pm 0.18 \pm 0.08$	$0.11^{+0.20}_{-0.08}^{+0.02}_{-0.01}$	$-0.03^{+0.07}_{-0.07}^{+0.01}_{-0.01}$
14.18 – 16.00	148 ± 13	$2.07 \pm 0.20 \pm 0.08$	$0.08^{+0.28}_{-0.08}^{+0.02}_{-0.01}$	$-0.01^{+0.12}_{-0.06}^{+0.01}_{-0.01}$
16.00 – 18.00	141 ± 13	$1.77 \pm 0.18 \pm 0.09$	$0.18^{+0.22}_{-0.14}^{+0.01}_{-0.04}$	$-0.09^{+0.07}_{-0.09}^{+0.02}_{-0.01}$
18.00 – 22.00	114 ± 13	$0.78 \pm 0.10 \pm 0.04$	$0.14^{+0.31}_{-0.14}^{+0.01}_{-0.02}$	$0.02^{+0.11}_{-0.11}^{+0.01}_{-0.01}$
1.00 – 6.00	357 ± 21	$2.41 \pm 0.17 \pm 0.14$	$0.05^{+0.08}_{-0.05}^{+0.04}_{-0.02}$	$0.02^{+0.05}_{-0.03}^{+0.02}_{-0.01}$

bins. The uncertainties coming from the corrections used to calibrate the performance of the simulation to match that of the data are at the level of 1 – 2%. The uncertainties on these corrections are limited by the size of the $D^{*+} \rightarrow D^0(\rightarrow K^- \pi^+) \pi^+$ and $J/\psi \rightarrow \mu^+ \mu^-$ control samples that are used to estimate the particle identification and tracking performance in the data. The signal and background mass models are also explored as a source of possible systematic uncertainty. In the fit to the $K^+ \mu^+ \mu^-$ invariant mass it is assumed that the signal line-shape is the same as that of the $B^+ \rightarrow K^+ J/\psi$ decay. In the simulation, small differences are seen in the B^+ mass resolution due to the different daughter kinematics between low and high q^2 . A 4% variation of the mass resolution is considered as a source of uncertainty and the effect on the result found to be negligible.

For the extraction of A_{FB} and F_{H} , the largest sources of uncertainty are associated with the event weights that are used to correct for the detector acceptance. The event weights are estimated from the simulation in $0.5 \text{ GeV}^2/c^4$ wide q^2 bins (driven by the size of the simulated event sample). At low q^2 , the acceptance variation can be large (at extreme values of $\cos \theta_\ell$) over the q^2 bin size. The order of the uncertainty associated with this binning is estimated by varying the event weights by half the difference between neighbouring q^2 bins and forms the dominant source of systematic uncertainty. The size of these effects on A_{FB} and F_{H} are at the level of 0.01 – 0.03 and 0.01 – 0.05 respectively, and are small compared to the statistical uncertainties. Variations of the background mass model are found to have a negligible impact on A_{FB} and F_{H} .

The background angular model is cross-checked by fitting a template to the angular distribution in the upper mass sideband and fixing this shape in the fit for A_{FB} and F_{H} in the signal mass window. This yields consistent results in every q^2 bin. Therefore, no systematic uncertainty is assigned to the background angular model. Two further cross checks have been performed. Firstly, A_{FB} has been determined by counting the number of forward- and backward-going events, after subtracting the background. Secondly, F_{H} has

been measured by fitting the $|\cos\theta_\ell|$ distribution, which is independent of A_{FB} . Consistent results are found in both cases.

7 Conclusions

The measured values of A_{FB} and F_{H} are consistent with the SM expectations of no forward-backward asymmetry and $F_{\text{H}} \sim 0$. The differential branching fraction of the $B^+ \rightarrow K^+\mu^+\mu^-$ decay is, however, consistently below the SM prediction at low q^2 . The results are in good agreement with, but statistically more precise than, previous measurements of $d\mathcal{B}/dq^2$ and A_{FB} from BaBar [35], Belle [36] and CDF [37]. Integrating the differential branching fraction, over the full q^2 range, yields a total branching fraction of $(4.36 \pm 0.15 \pm 0.18) \times 10^{-7}$, which is more precise than the current world average of $(4.8 \pm 0.4) \times 10^{-7}$ [26].

Acknowledgements

We express our gratitude to our colleagues in the CERN accelerator departments for the excellent performance of the LHC. We thank the technical and administrative staff at CERN and at the LHCb institutes, and acknowledge support from the National Agencies: CAPES, CNPq, FAPERJ and FINEP (Brazil); CERN; NSFC (China); CNRS/IN2P3 (France); BMBF, DFG, HGF and MPG (Germany); SFI (Ireland); INFN (Italy); FOM and NWO (The Netherlands); SCSR (Poland); ANCS (Romania); MinES of Russia and Rosatom (Russia); MICINN, XuntaGal and GENCAT (Spain); SNSF and SER (Switzerland); NAS Ukraine (Ukraine); STFC (United Kingdom); NSF (USA). We also acknowledge the support received from the ERC under FP7 and the Region Auvergne.

References

- [1] A. Ali, P. Ball, L. T. Handoko, and G. Hiller, *Comparative study of the decays $B \rightarrow (K, K^*)\ell^+\ell^-$ in the standard model and supersymmetric theories*, Phys. Rev. **D61** (2000) 074024, [arXiv:hep-ph/9910221](#).
- [2] C. Bobeth, G. Hiller, and G. Piranishvili, *Angular distributions of $\bar{B} \rightarrow K\bar{\ell}\ell$ decays*, JHEP **12** (2007) 040, [arXiv:0709.4174](#).
- [3] LHCb Collaboration, R. Aaij *et al.*, *Differential branching fraction and angular analysis of the decay $B^0 \rightarrow K^{*0}\mu^+\mu^-$* , Phys. Rev. Lett. **108** (2012) 181806, [arXiv:1112.3515](#); LHCb collaboration, *Differential branching fraction and angular analysis of the $B^0 \rightarrow K^{*0}\mu^+\mu^-$ decay*, LHCb-CONF-2012-008.
- [4] A. K. Alok, A. Dighe, and S. U. Sankar, *Large forward-backward asymmetry in $B \rightarrow K\mu^+\mu^-$ from new physics tensor operators*, Phys. Rev. **D78** (2008) 114025, [arXiv:0810.3779](#).

- [5] A. Khodjamirian, T. Mannel, A. A. Pivovarov, and Y.-M. Wang, *Charm-loop effect in $B \rightarrow K^{(*)}\ell^+\ell^-$ and $B \rightarrow K^*\gamma$* , JHEP **09** (2010) 089, [arXiv:1006.4945](#).
- [6] C. Bobeth, G. Hiller, D. van Dyk, and C. Wacker, *The decay $\bar{B} \rightarrow \bar{K}\ell^+\ell^-$ at low hadronic recoil and model-independent $\Delta B = 1$ constraints*, JHEP **01** (2012) 107, [arXiv:1111.2558](#).
- [7] LHCb collaboration, R. Aaij *et al.*, *Strong constraints on the rare decays $B_s \rightarrow \mu^+\mu^-$ and $B^0 \rightarrow \mu^+\mu^-$* , Phys. Rev. Lett. **108** (2012), [arXiv:1203.4493](#); CMS collaboration, S. Chatrchyan *et al.*, *Search for $B_s^0 \rightarrow \mu^+\mu^-$ and $B^0 \rightarrow \mu^+\mu^-$ decays*, JHEP **04** (2012) 033, [arXiv:1203.3976](#).
- [8] W. Altmannshofer, P. Paradisi, and D. M. Straub, *Model-independent constraints on new physics in $b \rightarrow s$ transitions*, JHEP **04** (2012) 008, [arXiv:1111.1257](#).
- [9] W. Altmannshofer and D. M. Straub, *Cornering new physics in $b \rightarrow s$ transitions*, JHEP **08** (2012) 121, [arXiv:1206.0273](#).
- [10] LHCb collaboration, R. Aaij *et al.*, *Measurement of the isospin asymmetry in $B \rightarrow K^{(*)}\mu^+\mu^-$ decays*, JHEP **07** (2012) 133, [arXiv:1205.3422](#).
- [11] LHCb collaboration, A. A. Alves Jr. *et al.*, *The LHCb detector at the LHC*, JINST **3** (2008) S08005.
- [12] T. Sjöstrand, S. Mrenna, and P. Skands, *PYTHIA 6.4 Physics and manual*, JHEP **05** (2006) 026, [arXiv:hep-ph/0603175](#).
- [13] I. Belyaev *et al.*, *Handling of the generation of primary events in GAUSS, the LHCb simulation framework*, Nuclear Science Symposium Conference Record (NSS/MIC) **IEEE** (2010) 1155.
- [14] D. J. Lange, *The EvtGen particle decay simulation package*, Nucl. Instrum. Meth. **A462** (2001) 152.
- [15] P. Golonka and Z. Was, *PHOTOS Monte Carlo: a precision tool for QED corrections in Z and W decays*, Eur. Phys. J. **C45** (2006) 97, [arXiv:hep-ph/0506026](#).
- [16] GEANT4 collaboration, J. Allison *et al.*, *Geant4 developments and applications*, IEEE Trans. Nucl. Sci. **53** (2006) 270; GEANT4 collaboration, S. Agostinelli *et al.*, *GEANT4: A simulation toolkit*, Nucl. Instrum. Meth. **A506** (2003) 250.
- [17] M. Clemencic *et al.*, *The LHCb simulation application, GAUSS: design, evolution and experience*, J. of Phys: Conf. Ser. **331** (2011) 032023.
- [18] V. V. Gligorov, *A single track HLT1 trigger*, LHCb-PUB-2011-003.
- [19] V. V. Gligorov, C. Thomas, and M. Williams, *The HLT inclusive B triggers*, LHCb-PUB-2011-016.

- [20] L. Breiman, J. H. Friedman, R. A. Olshen, and C. J. Stone, *Classification and regression trees*, Wadsworth international group, Belmont, California, USA, 1984.
- [21] Y. Freund and R. E. Schapire, *A decision-theoretic generalization of on-line learning and an application to boosting*, Jour. Comp. and Syst. Sc. **55** (1997) 119.
- [22] R. Forty, *RICH pattern recognition for LHCb*, Nucl. Instrum. Meth. **A433** (1999) 257.
- [23] BaBar Collaboration, B. Aubert *et al.*, *Evidence for direct CP violation from Dalitz-plot analysis of $B^\pm \rightarrow K^\pm \pi^\mp \pi^\pm$* , Phys. Rev. **D78** (2008) 012004, arXiv:0803.4451.
- [24] LHCb collaboration, *First observation of the decay $B^+ \rightarrow \pi^+ \mu^+ \mu^-$* , LHCb-PAPER-2012-020; LHCb collaboration, *First observation of $B^+ \rightarrow \pi^+ \mu^+ \mu^-$* , LHCb-CONF-2012-006.
- [25] T. Skwarnicki, *A study of the radiative cascade transitions between the Upsilon-prime and Upsilon resonances*, PhD thesis, Institute of Nuclear Physics, Krakow, 1986, DESY-F31-86-02.
- [26] Particle Data Group, J. Beringer *et al.*, *Review of particle physics*, Phys. Rev. **D86** (2012) 010001.
- [27] C. Bobeth, G. Hiller, and D. van Dyk, *More benefits of semileptonic rare B decays at low recoil: CP violation*, JHEP **07** (2011) 067, arXiv:1105.0376.
- [28] M. Beneke, T. Feldmann, and D. Seidel, *Systematic approach to exclusive $B \rightarrow V \ell^+ \ell^-$, $V \gamma$ decays*, Nucl. Phys. **B612** (2001) 25, arXiv:hep-ph/0106067.
- [29] B. Grinstein and D. Pirjol, *Exclusive rare $B \rightarrow K^* \ell^+ \ell^-$ decays at low recoil: controlling the long-distance effects*, Phys. Rev. **D70** (2004) 114005, arXiv:hep-ph/0404250.
- [30] M. Beylich, G. Buchalla, and T. Feldmann, *Theory of $B \rightarrow K^{(*)} \ell^+ \ell^-$ decays at high q^2 : OPE and quark-hadron duality*, Eur. Phys. J. **C71** (2011) 1635, arXiv:1101.5118.
- [31] P. Ball and R. Zwicky, *New results on $B \rightarrow \pi, K, \eta$ decay form factors from light-cone sum rules*, Phys. Rev. **D71** (2005) 014015, arXiv:hep-ph/0406232.
- [32] U. Egede *et al.*, *New observables in the decay mode $\bar{B}_d \rightarrow \bar{K}^{*0} \ell^+ \ell^-$* , JHEP **11** (2008) 032, arXiv:0807.2589.
- [33] A. Ali, E. Lunghi, C. Greub, and G. Hiller, *Improved model independent analysis of semileptonic and radiative rare B decays*, Phys. Rev. **D66** (2002) 034002, arXiv:hep-ph/0112300.
- [34] G. J. Feldman and R. D. Cousins, *Unified approach to the classical statistical analysis of small signals*, Phys. Rev. **D57** (1998) 3873, arXiv:physics/9711021.

- [35] BaBar collaboration, B. Aubert *et al.*, *Measurements of branching fractions, rate asymmetries, and angular distributions in the rare decays $B \rightarrow K\ell^+\ell^-$ and $B \rightarrow K^*\ell^+\ell^-$* , Phys. Rev. **D73** (2006) 092001, [arXiv:hep-ex/0604007](#); BaBar collaboration, J. P. Lees *et al.*, *Measurement of branching fractions and rate asymmetries in the rare decays $B \rightarrow K^{(*)}\ell^+\ell^-$* , [arXiv:1204.3933](#).
- [36] Belle collaboration, J.-T. Wei *et al.*, *Measurement of the differential branching fraction and forward-backward asymmetry for $B \rightarrow K^{(*)}\ell^+\ell^-$* , Phys. Rev. Lett. **103** (2009) 171801, [arXiv:0904.0770](#).
- [37] CDF collaboration, T. Aaltonen *et al.*, *Measurements of the angular distributions in the decays $B \rightarrow K^{(*)}\mu^+\mu^-$ at CDF*, Phys. Rev. Lett. **108** (2012) 081807, [arXiv:1108.0695](#).